Geophys. J. Int. (2008) **173,** 566–576 doi: 10.1111/j.1365-246X.2008.03747.x

Monte Carlo simulation of radiative energy transfer in continuous elastic random media—three-component envelopes and numerical validation

Jens Przybilla and Michael Korn

Institute for Geophysics and Geology, University of Leipzig, Talstraße 35, D-04103 *Leipzig, Germany. E-mail: mikorn@uni-leipzig.de*

Accepted 2008 January 29. Received 2008 January 29; in original form 2007 August 8

SUMMARY

We present Monte Carlo solutions of the 3-D radiative transfer (RT) equations for energy transport in elastic media with randomly fluctuating velocity and density. It includes mode conversions from *P*- to *S*-wave energy and vice versa and considers angular-dependent scattering patterns following from the Born approximation. Synthesis of the space–time distribution of seismic energy emitted from point sources with arbitrary radiation patterns can be achieved. The method offers a unique way to model complete mean square envelopes of high-frequency wavefields in the presence of random heterogeneity starting from the first *P*-wave onset until the late *S*-wave coda.

Validation of the method is achieved through a comparison of mean square envelopes from an isotropic *P*-wave radiation point source with full 3-D wavefield simulations for the whole envelope shape and with the analytical Markov approximation for small lapse times. RT yields accurate envelope shapes even for parameter ranges where strong and direction-dependent scattering occurs. Peak amplitudes, envelope broadening and coda decay at long lapse times are correctly modelled. A breakdown of RT with Born scattering coefficients only occurs in the vicinity of a point source: waveform modelling shows that even for a pure compressional source, some per cent of shear wave energy are generated by near-source scattering that are not explained within the framework of Born approximation.

Key words: Computational seismology; Theoretical seismology; Wave scattering and diffusion; Wave propagation.

GJI Seismology

Downloaded from https://academic.oup.com/gji/article/173/2/566/728673 by guest on 16 August 2022

1 INTRODUCTION

Short period wave propagation through the lithosphere results in complex wave trains that are mainly composed of waves multiply scattered at small-scale heterogeneities of the Earth medium. Often it is useful to disregard phase information and focus on bandpass filtered envelopes of recorded seismograms instead of the full waveforms, as envelopes are stable features that allow the retrieval of statistical parameters of the lithospheric heterogeneity where deterministic methods like tomography fail. Statistical parameters like rms velocity and density fluctuation, correlation distance or scattering attenuation are useful informations closely related to stratigraphy, stress distribution, crack density, pore fluids etc.

One of the most general methods to describe energy transport in scattering media is the radiative transfer theory (RTT). Originally, it was used in atmospheric sciences to describe the scattering of light in the atmosphere (Chandrasekar 1960). Only later it was introduced phenomenologically into seismology. Aki & Chouet (1975) proposed a single backscattering model to explain the generation of the seismic coda by seismic wave scattering at the heterogeneous structure of the Earth. Sato (1977) developed an isotropic single scattering model for arbitrary source–receiver configurations. Later Sato (1984) developed three-component envelope synthesis, based on the single-scattering approximation with Born scattering coefficients in random elastic media. Wu (1985) presented a RT method to separate scattering attenuation from intrinsic attenuation. Multiple scattering models were developed, for example, by Zeng *et al*. (1991), Hoshiba (1991) and Gusev & Abubakirov (1996). A strict derivation of RT from the linear elastic wave equation in random media could also be achieved (Rytov *et al*. 1987; Weaver 1990; Ryzhik *et al*. 1996).

For some special cases approximate analytical solutions of the RT equations exist, for example, for scalar waves and isotropic scattering (Paaschens 1997), which have been applied to the interpretation of *S*-wave coda from local events (Sens-Schönfelder & Wegler 2006; Padhy *et al*. 2007). For long lapse times and/or strong multiple scattering, RT approaches the diffusion equation. In more general cases, however, numerical solutions of the RT equations have to be considered. They are usually based on Monte Carlo schemes where a random walk of energy particles through the heterogeneous medium is realized. Each particle is moved along ballistic ray paths between individual scattering events. Gusev & Abubakirov (1987) and Hoshiba (1991) were among the first to use this method in seismology. Yoshimoto (2000) simulated seismogram envelopes for

© 2008 The Authors
Journal compilation © 2008 RAS

isotropic scattering and scalar waves in a background medium with a velocity gradient with depth, which can be implemented by moving the particles along curved ray trajectories between scattering events. Wegler *et al*. (2006) compared the performance of isotropic and non-isotropic scattering approximations for scalar waves and found that isotropic scattering yields considerable deviations in the early parts of the coda. Margerin *et al*. (2000), for the first time, developed a Monte Carlo scheme for the full elastic vector wave case in a medium with discrete scatterers, where conversions between *P*- and *S*-wave modes are taken into account, and the *S*-wave polarization is taken care of with the help of the Stokes vector. Elastic RT has been applied to deep mantle scattering (Margerin & Nolet 2003; Shearer & Earle 2004).

Przybilla *et al*. (2006) proposed a RT scheme for elastic vector waves in 2-D continuous random media employing angular-dependent scattering patterns described by Born scattering coefficients (Sato & Fehler 1998). They tested the accuracy of envelope shapes against averaged envelopes from full waveform modelling with a finite-difference (FD) method and found that RT yields accurate envelope shapes for a wide range of medium parameters, including strong forward scattering cases.

In this paper we extend the 2-D method of Przybilla *et al*. (2006) to three dimensions. We avoid introducing the Stokes vector and instead use the polarization decomposed Born scattering coefficients to carry the polarization information of *S*-wave particles across scattering events. The method enables us to model complete three-component mean square envelopes in random media with prescribed autocorrelation functions from the first *P* onset until the late *S* coda. Thus, this method is more powerful than diffusion approaches, which only model late *S* coda, and the Markov approximation, which is only valid around the ballistic direct wave arrivals, and more accurate than multiple scattering methods with isotropic scattering assumptions. We expect that by inverting complete seismogram envelopes, we will get more reliable information on the statistics of the propagation media than by using only scalar approximation to model the *S*-wave envelopes.

Similarly to Przybilla *et al*. (2006), we demonstrate the accuracy of our approach by comparing it to average envelope shapes from full 3-D elastic waveform modelling. We further compare the pulse broadening effect for strong forward scattering with the newly developed Markov approximation for vector waves (Sato 2007).

2 ELASTIC RADIATIVE TRANSFER THEORY

2.1 Basic equations

For a detailed derivation of RT equations from wave theory in random media, we refer to Ryzhik *et al*. (1996). The key quantity in this theory is the specific intensity $\boldsymbol{I}(\mathbf{x}, \mathbf{k}, t)$ of a wave at point $\mathbf{x}$, time t, moving in direction $\mathbf{k}$. Here we introduce specific intensities I^p and I^s for *P* and *S* waves, respectively. Following Ryzhik *et al*. (1996) the coupled elastic energy transfer equations for I^p and I^s can be written as

$$\begin{aligned}
&\frac{1}{\alpha_0}\frac{\partial I^P(\mathbf{x},\mathbf{k},t)}{\partial t} + \mathbf{k}\cdot\mathrm{grad} I^P(\mathbf{x},\mathbf{k},t)\\
&= \frac{1}{4\pi}\int g_{pp}(\mathbf{k},\mathbf{k}') I^P(\mathbf{x},\mathbf{k}',t)\,\mathrm{d}\mathbf{k}' - g_{pp}^0 I^P(\mathbf{x},\mathbf{k},t)\\
&+\frac{1}{4\pi}\int g_{sp}(\mathbf{k},\mathbf{k}') I^S(\mathbf{x},\mathbf{k}',t)\,\mathrm{d}\mathbf{k}' - g_{ps}^0 I^P(\mathbf{x},\mathbf{k},t) + Q^P(\mathbf{x},\mathbf{k},t)\\
&\frac{1}{\beta_0}\frac{\partial I^S(\mathbf{x},\mathbf{k},t)}{\partial t} + \mathbf{k}\cdot\mathrm{grad} I^S(\mathbf{x},\mathbf{k},t)\\
&= \frac{1}{4\pi}\int g_{ss}(\mathbf{k},\mathbf{k}') I^S(\mathbf{x},\mathbf{k}',t)\,\mathrm{d}\mathbf{k}' - g_{ss}^0 I^S(\mathbf{x},\mathbf{k},t)\\
&+\frac{1}{4\pi}\int g_{ps}(\mathbf{k},\mathbf{k}') I^P(\mathbf{x},\mathbf{k}',t)\,\mathrm{d}\mathbf{k}' - g_{sp}^0 I^S(\mathbf{x},\mathbf{k},t) + Q^S(\mathbf{x},\mathbf{k},t)\,. \qquad (1)
\end{aligned}$$

In eq. (1) unit wavenumber $\mathbf{k}$ denotes incident wave direction and $\mathbf{k}'$, any other direction. α_0 and β_0 are the mean *P* and *S* velocities. g_{ij} and $g_{ij}{}^0$ ($i, j = P$ or *S*) are angular-dependent and total scattering coefficients (see below), respectively. The left-hand side of eq. (1) represents the total time derivative of intensities and describes the intensity transport of *P* and *S* waves. The right-hand side contains the intensity loss from the direction of propagation into all other directions $\mathbf{k}'$ through the total scattering coefficients $g_{ij}{}^0$, and the intensity gain from all directions into the propagation direction $\mathbf{k}$ through the integral over g_{ij}. Conversion scattering between *P* and *S* energy is contained in g_{ps} and g_{sp} and couples both equations. $Q^{P,S}(\mathbf{x}, \mathbf{k}, t)$ represent sources of *P* and *S* waves.

The basic assumptions of RTT are: (1) fluctuations of the inhomogeneities are weak; (2) wavelength and correlation length of the heterogeneities are of comparable size and (3) phases of waves from different scattereres are independent of each other, that is, the energy of scattered wave packets can be stacked (Rhyzhik *et al*. 1996). This is often casted into the condition $(ka\varepsilon)^2 \ll 1$ (Apresyan & Kravtsov 1996, p. 184; Gusev & Abubakirov 1996). Energy dissipation and velocity dispersion are neglected in eq. (1).

2.2 Scattering coefficients

For determination of the scattering coefficients g_{ij} in eq. (1), we use the random medium model with continuous velocity and density fluctuations with respect to a constant background model α_0, β_0 and density ρ_0. Here we use the assumption (e.g. Sato & Fehler 1998, p. 101) that *P*- and *S*-wave velocity fluctuations are proportional to each other and that wave velocity and density follow a linear relationship (Birch 1961). Then the number of independent fractional fluctuations is reduced to one spatially stationary random variable $\xi(\mathbf{x})$:

$$\frac{\delta\alpha}{\alpha_0} = \frac{\delta\beta}{\beta_0} = \frac{1}{\nu}\frac{\delta\rho}{\rho_0} = \xi(\mathbf{x})\,. \qquad (2)$$

Useful values for ν are in the range 0.3–0.8. The statistics of the medium is given by the autocorrelation function

$$R(\mathbf{x}) = \langle \xi(\mathbf{x}+\mathbf{x}')\xi(\mathbf{x}')\rangle, \qquad (3)$$

and variance

$$\varepsilon^2 = R(0) = \langle \xi(\mathbf{x})^2\rangle. \qquad (4)$$

The power spectrum of the medium at wavenumber $\mathbf{m}$ is obtained by a Fourier transform of *R* as

$$P(\mathbf{m}) = \int\int\int R(\mathbf{x})\mathrm{e}^{-i\mathbf{m}\cdot\mathbf{x}}\mathrm{d}\mathbf{x}. \qquad (5)$$

Coefficients g_{ij} describe single scattering interactions of wave packets with the random heterogeneities and can be obtained within the framework of Born approximation (e.g. Sato & Fehler 1998, p. 95ff). Many previous RT solutions have assumed average, direction-independent values for these coefficients. Although this is a reasonable assumption in the Rayleigh scattering domain when the correlation distance of heterogeneities is much smaller than the

Downloaded from https://academic.oup.com/gji/article/173/2/566/728673 by guest on 16 August 2022

wavelength ($ak \ll 1$), it becomes obsolete for correlation distance larger than the wavelength ($ak \geq 1$). In this case, scattering is dominant in near to forward directions.

Here, we use the complete direction dependent Born scattering coefficients as given by Sato & Fehler (1998). We repeat them for completeness.

$$g_{pp}(\theta,\varphi) = \frac{k_s^4}{4\pi}\left|X_r^{pp}(\theta,\varphi)\right|^2 P\left(\frac{2k_s}{\gamma_0}\sin\frac{\theta}{2}\right)$$

$$g_{ps}(\theta,\varphi) = \frac{k_s^4}{4\pi\gamma_0}\left|X_\theta^{ps}(\theta,\varphi)\right|^2 P\left(\frac{k_s}{\gamma_0}\sqrt{1+\gamma_0^2-2\gamma_0\cos\theta}\right)$$

$$g_{sp}(\theta,\varphi) = \frac{\gamma_0 k_s^4}{4\pi}\left|X_r^{sp}(\theta,\varphi)\right|^2 P\left(\frac{k_s}{\gamma_0}\sqrt{1+\gamma_0^2-2\gamma_0\cos\theta}\right) \tag{6}$$

$$g_{ss}(\theta,\varphi) = g_{ss_\theta}(\theta,\varphi) + g_{ss_\varphi}(\theta,\varphi),$$

where g_{ss} is further split into two components orthogonal polarization:

$$g_{ss_\varphi}(\theta,\varphi) = \frac{k_s^4}{4\pi}\left|X_\varphi^{ss}(\theta,\varphi)\right|^2 P\left(2k_s\sin\frac{\theta}{2}\right)$$

$$g_{ss_\theta}(\theta,\varphi) = \frac{k_s^4}{4\pi}\left|X_\theta^{ss}(\theta,\varphi)\right|^2 P\left(2k_s\sin\frac{\theta}{2}\right) \tag{7}$$

Here k_s is the wavenumber of S waves and $\gamma_0 = \alpha_0/\beta_0$.

The basic radiation patterns X_{ij} are given by

$$X_r^{pp}(\theta,\varphi) = \gamma_0^{-2}\left[\nu\left(\cos\theta + 2\gamma_0^{-2}\sin^2\theta - 1\right) - 2 + 4\gamma_0^{-2}\sin^2\theta\right]$$

$$X_\theta^{ps}(\theta,\varphi) = -\sin\theta\left[\nu\left(2\gamma_0^{-1}\cos\theta - 1\right) - 4\gamma_0^{-1}\cos\theta\right]$$

$$X_r^{sp}(\theta,\varphi) = \gamma_0^{-2}\sin\theta\cos\varphi\left[\nu\left(1 - 2\gamma_0^{-1}\cos\theta\right) - 4\gamma_0^{-2}\cos\theta\right]$$

$$X_\theta^{ss}(\theta,\varphi) = \cos\varphi\left[\nu\left(\cos\theta - \cos 2\theta\right) - 2\cos 2\theta\right]$$

$$X_\varphi^{ss}(\theta,\varphi) = \sin\varphi\left[\nu\left(\cos\theta - 1\right) + 2\cos\theta\right]. \tag{8}$$

See Fig. 1 for the definition of angles θ and φ in a local Cartesian coordinate system, where the incident wave moves into x_3-direction and S-wave polarization is in x_1-direction.

The average of g_{ij} over the solid angle gives the total scattering coefficients ${g_{ij}}^0$ (e.g. Sato & Fehler 1998, p. 43).

2.3 Monte Carlo solution of radiative transfer equation

It is common practise to solve the RT equation by a Monte Carlo method (e.g. Margerin *et al.* 2000; Yoshimoto 2000). Energy transport is described by wave packets or particles emitted from the source in direction **k** with linear polarization **p**. Each particle moves along a ballistic path until it experiences a scattering event. Scattering changes the propagation direction and eventually the wave mode. The average distance between two scattering events is determined from mean free path lengths l_p and l_s.

Here we consider a P-wave source at the origin of a global Cartesian coordinate system (x, y, z) with isotropic source radiation. Initial

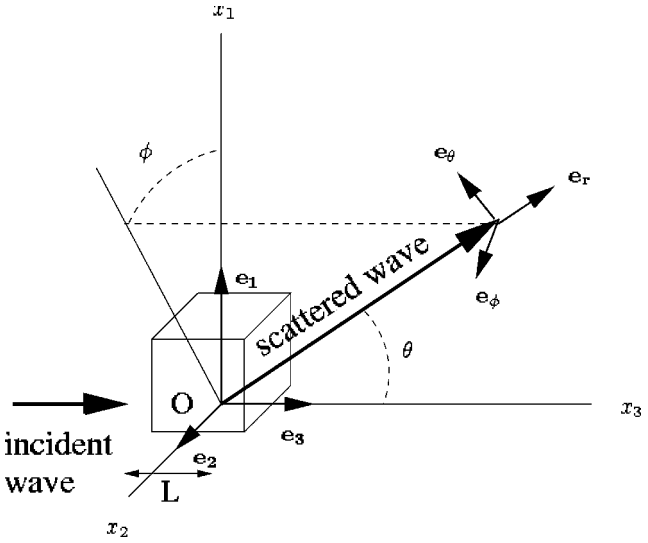

Figure 1. Local Cartesian coordinate system (x_1, x_2, x_3) with incident wave direction $\mathbf{k} = \mathbf{e_3}$ and scattering angles θ and φ. For incident P wave, polarization is $\mathbf{p} = \mathbf{e_3}$ and for incident S wave, $\mathbf{p} = \mathbf{e_1}$.

direction **k** of the particles is determined by

$$\mathbf{k} = \begin{pmatrix} \cos\varphi'\sin\theta' \\ \sin\varphi'\sin\theta' \\ \cos\theta' \end{pmatrix} \tag{9}$$

with

$$\theta' = \arccos(1 - 2Z_1),$$
$$\varphi' = 2\pi Z_2, \tag{10}$$

where $Z_{1,2}$ are uniform random numbers between 0 and 1, and $\mathbf{p} = \mathbf{k}$. Different source characteristics could be obtained by appropriate choice of Q^p and Q^s in eq. 1.

Mean free path length between two successive scattering interactions is related to the total scattering coefficients as (Ryzhik *et al.* 1996)

$$l_p = \left(g_{pp}^0 + g_{ps}^0\right)^{-1}$$
$$l_s = \left(g_{ss_\theta}^0 + g_{ss_\varphi}^0 + g_{sp}^0\right)^{-1}. \tag{11}$$

Particles are moved in small time steps $\mathrm{d}t = l_s/(10v_p)$. Probability P that scattering of a P or S particle takes place within $\mathrm{d}t$ is given by

$$P(P,S) = 1 - \exp(\alpha_0 \mathrm{d}t / l_{P,S}). \tag{12}$$

When a scattering event takes place, the new wave mode is determined first. To keep complete polarization information, we distinguish between two S-wave modes with linear polarization perpendicular to each other, which are denoted by angles θ and φ in the local Cartesian coordinate system (Fig. 1).

Probabilities Π for scattering between each mode are determined from the total scattering coefficients and mean free paths as follows:

$$\Pi_{PP} = g_{pp}^0 l_p,$$
$$\Pi_{PS_\theta} = g_{ps}^0 l_p,$$
$$\Pi_{SP} = g_{sp}^0 l_s,$$
$$\Pi_{SS_\theta} = g_{ss_\theta}^0 l_s,$$
$$\Pi_{SS_\varphi} = g_{ss_\varphi}^0 l_s. \tag{13}$$

Downloaded from https://academic.oup.com/gji/article/173/2/566/728673 by guest on 16 August 2022

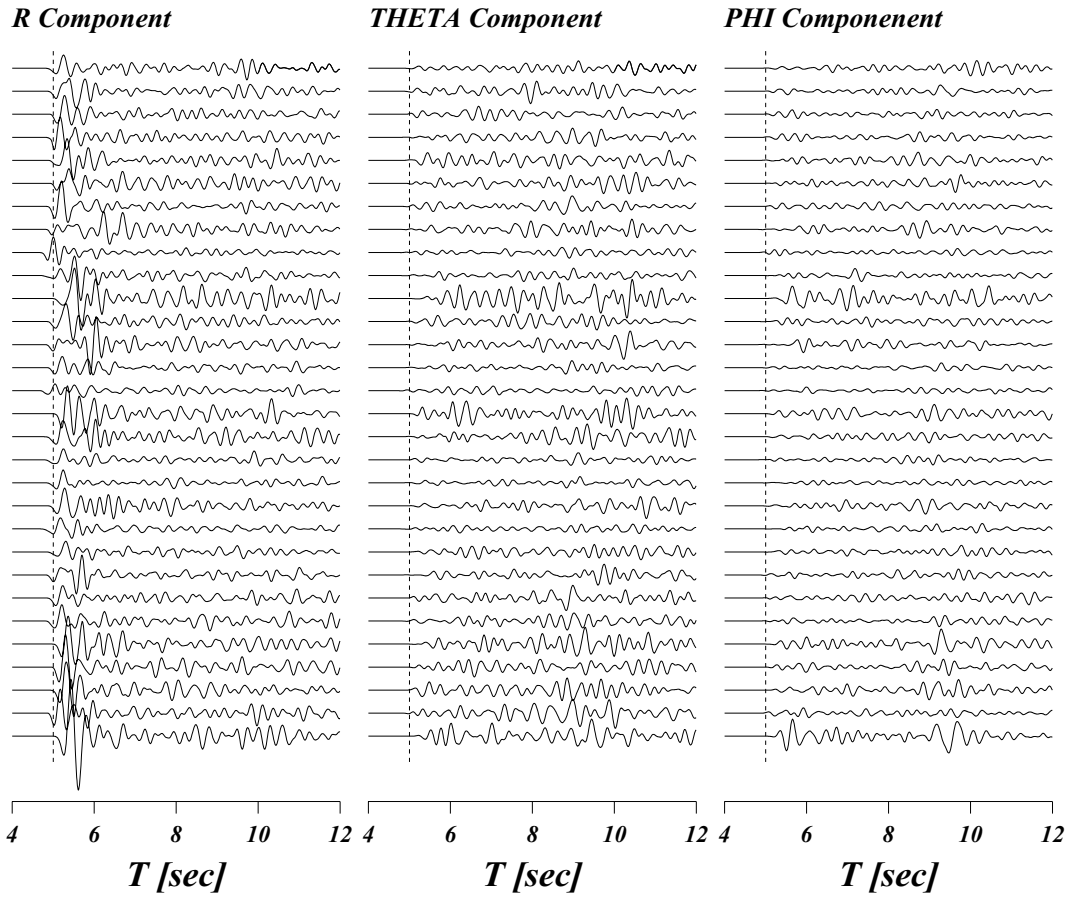

Figure 2. Finite difference traces at 30 km distance from the source in an exponential random medium with $ak = 3.14$. The dashed vertical line indicates the arrival time of a *P* wave travelling with the average velocity of the random medium.

Finally, scattering direction is determined from the angular-dependent scattering coefficients (eq. 6). Probabilities of scattering into angles θ, φ are given by (Modest 1993)

$$Z_3 = 1 - \int_0^{\theta} \int_0^{2\pi} \frac{g_{ij}(\theta', \varphi')}{g_{ij}^0} \sin\theta' \, \mathrm{d}\theta' \, \mathrm{d}\varphi'$$
$$Z_4 = 1 - \int_0^{\varphi} \int_0^{\pi} \frac{g_{ij}(\theta', \varphi')}{g_{ij}^0} \sin\theta' \, \mathrm{d}\theta' \, \mathrm{d}\varphi', \tag{14}$$

where Z_3 and Z_4 are uniform random numbers. Eq. (14) have to be solved numerically for angles θ, φ. This is done once at the beginning of the calculations and the results are stored in tables to speed up computing time. The integration steps $\Delta\theta$, $\Delta\varphi$ are chosen such that each interval represents equal probability, for example,

$$\int_{\theta}^{\theta+\Delta\theta} \int_0^{2\pi} \frac{g_{ij}(\theta', \varphi')}{g_{ij}^0} \sin\theta' \, \mathrm{d}\theta' \, \mathrm{d}\varphi' = \frac{1}{q}. \tag{14a}$$

Here we use $q = 10\,000$. Then the resolution is fine enough for narrow indicatrices. For more details see Lux & Koblinger (1991) and Margerin *et al.* (2000).

After the scattering process, the new propagation direction is given by

$$\mathbf{k_1} = \begin{pmatrix} \cos\varphi \sin\theta \\ \sin\varphi \sin\theta \\ \cos\theta \end{pmatrix} \tag{15}$$

and polarization is

$$\mathbf{p_P} = \mathbf{k_1},$$
$$\mathbf{p_{S_\theta}} = \begin{pmatrix} \cos\theta \cos\varphi \\ \cos\theta \sin\varphi \\ -\sin\theta \end{pmatrix}, \tag{16}$$
$$\mathbf{p_{S_\varphi}} = \begin{pmatrix} -\sin\varphi \\ \cos\varphi \\ 0 \end{pmatrix}$$

depending on the wave mode. Finally, these directions are rotated back into the global coordinate system and carried with the particle until the next scattering event.

All particles passing through the volume V of a spherical shell with radius R and thickness $\mathrm{d}R$ contribute to the energy density at a receiver point at distance R at their time of passage. An appropriate value of $\mathrm{d}R$ depends on the mean free path with $\mathrm{d}R = v_p \mathrm{d}t$ for *P* particles and $\mathrm{d}R = v_S \, \mathrm{d}t$ for *S* particles.

Total energy density at distance R and time t_i is then given by the number of particles passing through V at time step t_i as

$$E(R, t_i) = \frac{N(R, t_i)}{N_0 V}, \tag{17}$$

where N_0 is the total number of particles in the simulation. Component-resolved energy density is obtained from the polarization and propagation vectors carried with each particle.

© 2008 The Authors, *GJI*, **173,** 566–576
Journal compilation © 2008 RAS

Downloaded from https://academic.oup.com/gji/article/173/2/566/728673 by guest on 16 August 2022

3 FINITE-DIFFERENCE SIMULATIONS IN 3-D ELASTIC MEDIA

3.1 Method

For the computation of theoretical waveforms of vector waves in 3-D random media, we employ a FD technique based on a staggered-grid approach for particle velocities and stresses in space–time domain. The accuracy is second-order in time and fourth-order in space. We use a parallel implementation of the scheme developed by Bohlen (2002), which makes use of domain decomposition and runs on PC clusters or on massive parallel supercomputers using the Message Passing Interface (MPI) standard.

The size of the model is $76 \times 76 \times 76$ km. Mean P and S velocities are $\alpha_0 = 6$ km s^{-1}, and $\beta_0 = -3.46$ km s^{-1}. A random fractional velocity fluctuation $\xi(\mathbf{x})$ with exponential ACF

$$R_e(\mathbf{x}) \equiv R_e(r) = \langle \xi(\mathbf{x}')\,\xi(\mathbf{x}'+\mathbf{x}) \rangle = \varepsilon^2 \mathrm{e}^{-r/a}, \tag{18}$$

or Gaussian ACF

$$R_g(\mathbf{x}) \equiv R_g(r) = \langle \xi(\mathbf{x}')\,\xi(\mathbf{x}'+\mathbf{x}) \rangle = \varepsilon^2 \mathrm{e}^{-r^2/a^2}, \tag{19}$$

with $r = \sqrt{x^2+y^2+z^2}$ is imposed on both P and S velocities. Parameter ε is rms fractional fluctuation and a is correlation distance. Density perturbations are assumed to be totally correlated with velocity fluctuations and $\nu = 0.8$(see eq. 2).

A compressional source with isotropic radiation pattern is located at the centre of the model. The time dependence of source stress is given by

$$f(t) = \sin(2\pi t/T) - \frac{1}{2}\sin(4\pi t/T) \quad 0 \le t \le T, \tag{20}$$

where T is the duration of the wavelet. The far-field pulse shape is then $u_{\mathrm{far}}(t) \propto \frac{\mathrm{d}f}{\mathrm{d}t}$. Here we choose $T = 0.5$ s to obtain a wavelet with a dominant frequency of about 3 Hz. The wavefield is recorded on spheres at distances of 10, 20 and 30 km from the source. On each sphere, receivers are separated by approximately 2.6 km from one another. This yields a total number of 186, 745 and 1675 receivers at the three distances. The spatial and temporal discretization in the FD scheme is 0.1 km and 6 ms, respectively. This choice ensures that the numerical errors remain small.

At the boundaries of the computational grid, exponential damping (Cerjan *et al*. 1985) is applied to achieve non-reflecting boundaries. Nevertheless, the presence of artificial boundaries introduces errors by generating weak spurious reflections and suppressing backward scattering from the area outside the grid. Due to the limitations in computing resources these cannot be avoided by making the grid larger.

Numerical simulations have been performed for correlation distances a of 1 and 3 km. This corresponds to $ak = 3.14$ and 9.42, respectively, where k is S wavenumber at the dominant frequency. Due to the limited propagation distance, we had to take a rather large value of rms fluctuation $\varepsilon = 10$ per cent to generate significant scattered energy. One simulation took about 3 hr wall clock time on the IBM p690-Cluster JUMP at Forschungszentrum Jülich using 512 processing elements.

In Fig. 2, individual traces at 30 km distance from the source are displayed for exponential ACF and $ak = 3.14$. Severe pulse shape distortions and amplitude fluctuations are observed, together with coda excitation in all three components. Note that traveltime fluctuations of the first onset are clearly visible, and first arrivals of the radial component sometimes travel faster than the average velocity of the random medium. This effect is well known (e.g. Witte *et al*. 1996), but will not be present in RT envelopes as all particles strictly move with the average velocity.

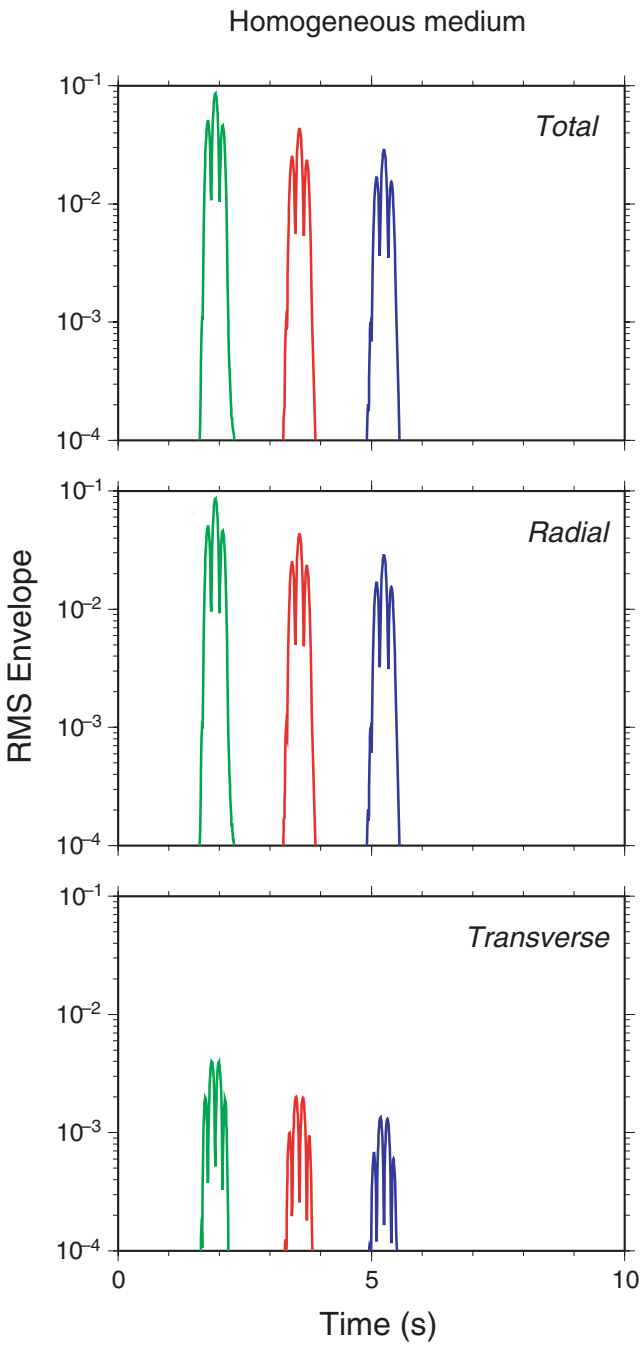

Figure 3. Root mean squared (rms) envelopes from finite difference calculations in a homogeneous medium. Note the shape of the P pulse, the absence of energy at S arrival time and the appearance of a small transverse component. Only one transverse component is shown, as the other one is almost identical. Colours correspond to travel distances of 10 km (green), 20 km (red) and 30 km (blue).

3.2 RMS envelopes

For the comparison with theoretical envelopes from RT and Markov theory, the following data processing was done: rotation of original components into radial and transverse components; stacking of the

Downloaded from https://academic.oup.com/gji/article/173/2/566/728673 by guest on 16 August 2022

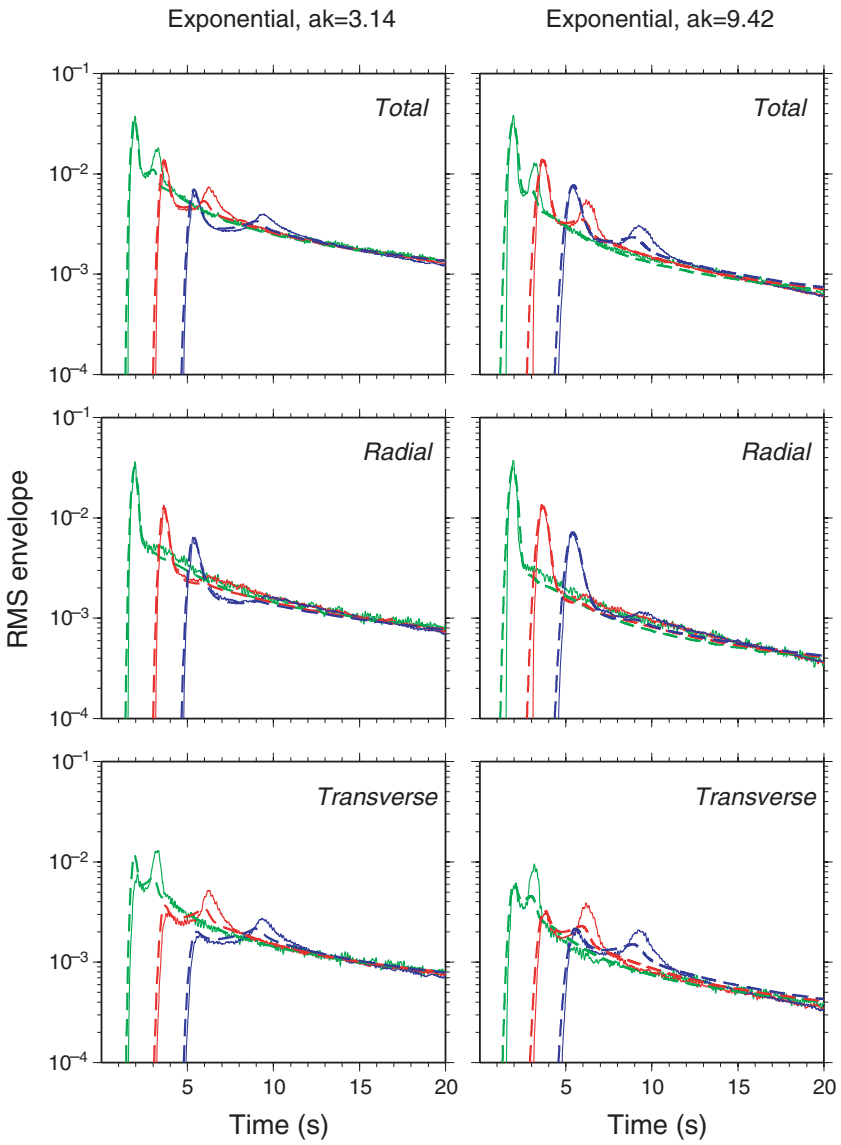

Figure 4. The rms envelopes in a medium with exponential autocorrelation function, $\varepsilon = 10$ per cent, and correlation length $a = 1$ km (left) and 3 km (right). The dashed lines are the RT envelopes; FD envelopes are plotted with solid lines.

squared single-component traces of all receivers at a fixed travel distance to obtain average MS envelopes; summing of all components to obtain total MS envelope. For some comparisons, an additional Gaussian bandpass filter has been applied as the first processing step. This is explained later.

In Fig. 3, we show the rms envelopes obtained from a simulation in a homogeneous medium. The envelope shape as $u^2_{\rm far}$ is clearly recognized in the total and radial components. The transverse component, which theoretically should be zero, shows a small amplitude of about 4 per cent and a distorted pulse shape. This is due to the well-known effects of numerical grid dispersion and grid anisotropy in the FD scheme, and gives an idea about the accuracy limit of the numerical simulations. We note that there is only energy at the *P* arrival time, and that the source does not emit any *S* waves.

Before comparing the envelopes obtained by RT or Markov theory with the averaged FD envelopes, two more processing steps have to be done. In FD, the outgoing wavelet has a pulse shape of finite length whereas in the RT and Markov, a spike-like source time function is assumed. Before a quantitative comparison, RT and Markov MS envelopes have to be convolved with the squared FD wavelet $u^2_{\rm far}(t)$.

The second difference is that during propagation through a random medium, the wave fronts become distorted and exhibit travel-time fluctuations. When averaging over many observation points as was done in the FD calculations, one has the choice of either aligning the individual traces before stacking or not. The second choice, which we use here, yields a pulse broadening in the resulting envelope, which is additional to the broadening observed in individual traces in the case of strong forward scattering. To take this into account, we may use the wandering effect (Lee & Jokipii 1975; Sato & Fehler 1998). It serves as an additional convolution operator for the RT and Markov envelopes. The wandering effect is given as

$$w(r,t) = \frac{v_0}{\sqrt{2\pi A(0) r}} \mathrm{e}^{-\frac{v_0^2 r^2}{2A(0)r}}, \qquad (21)$$

© 2008 The Authors, *GJI*, **173,** 566–576
Journal compilation © 2008 RAS

Downloaded from https://academic.oup.com/gji/article/173/2/566/728673 by guest on 16 August 2022

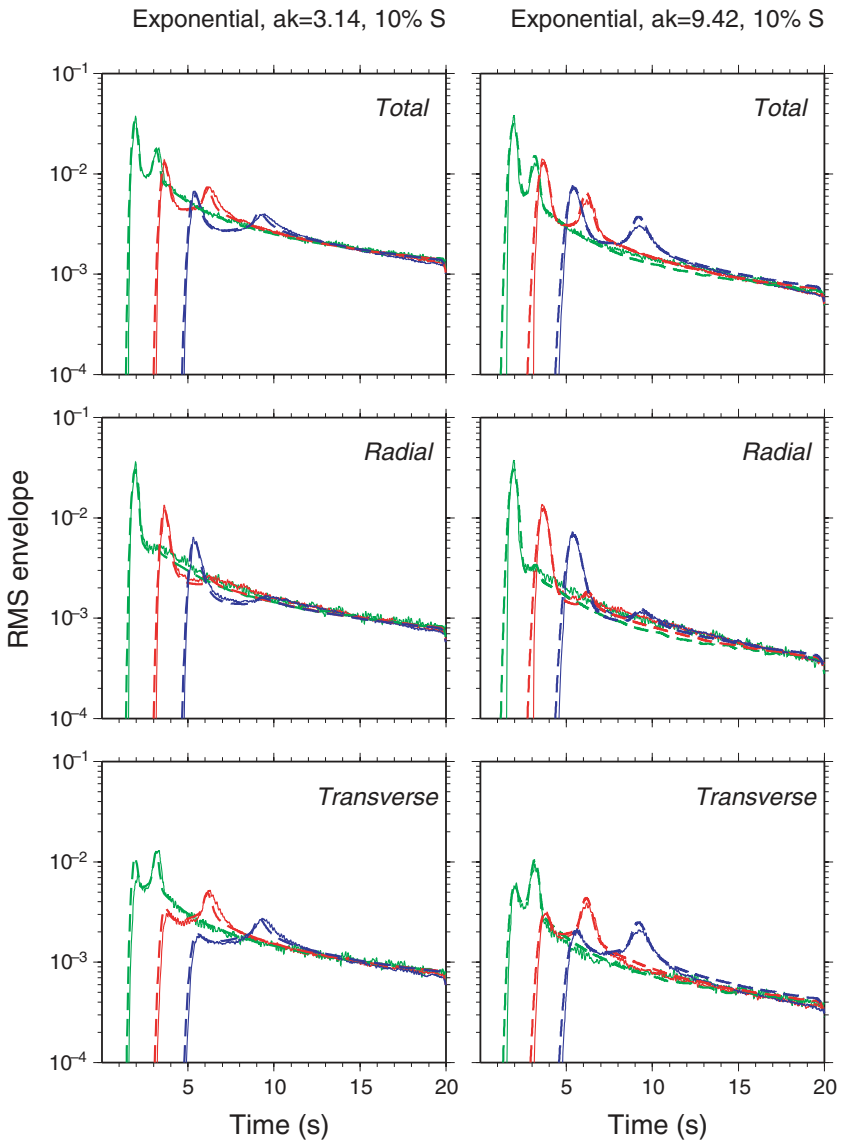

Figure 5. Same as Fig. 4, but with 10 per cent additional *S* energy emitted by the RT source.

where r is propagation distance and A is the longitudinal integral of the ACF (Sato & Fehler 1998):

$$A\,(x=0,z) \equiv \int_0^\infty R(x=0,z) \quad \mathrm{d}z = \begin{cases} \sqrt{\pi}\varepsilon^2 a \text{ Gaussian} \\ 2\varepsilon^2 a \text{ Exponential} \end{cases} . \quad (22)$$

Strictly speaking, the application of eq. (21) is only correct for the time interval of the direct wave arrival, but we found that there is little effect on the later parts of the envelope due to their smooth behaviour with time.

It is worth mentioning that the wandering effect should not be used if single trace envelopes are compared with RT or Markov simulations or if traces have been time aligned before stacking.

4 MONTE CARLO VERSUS FD ENVELOPES

In Fig. 4, the comparison between total, radial and transverse component rms envelopes obtained from RT and FD simulations is shown for a random medium with exponential ACF and $\varepsilon = 0.1$. Correlation distance is 1 km (left-hand side) and 3 km (right-hand side) resulting in values of $ak = 3.14$ and 9.42, respectively. This covers the range of moderate to strong forward scattering where the angular dependence of the scattering coefficients becomes increasingly important. For larger ak values the pulse broadening due to forward scattering becomes larger and the later coda generated by multiple large-angle scattering becomes smaller. In all simulations we show only one transverse component, as the other is practically identical, as can be expected. MS envelopes from RT have been convolved with the squared source signal and the wandering effect.

In both cases, the results of RT and FD agree reasonably well in amplitude and pulse shape around the *P*-wave arrival and also in the later part of the coda. A slightly higher decay rate of the FD envelopes can be explained by the finite dimension of the numerical model. Once the initial wave front hits the boundaries, it is absorbed and further large-angle and backscattering is suppressed resulting in some missing energy at late times in the FD coda.

The main difference between FD and RT occurs around 3, 6 and 9 s at distances 10, 20 and 30 km, respectively, in the transverse (and

Downloaded from https://academic.oup.com/gji/article/173/2/566/728673 by guest on 16 August 2022

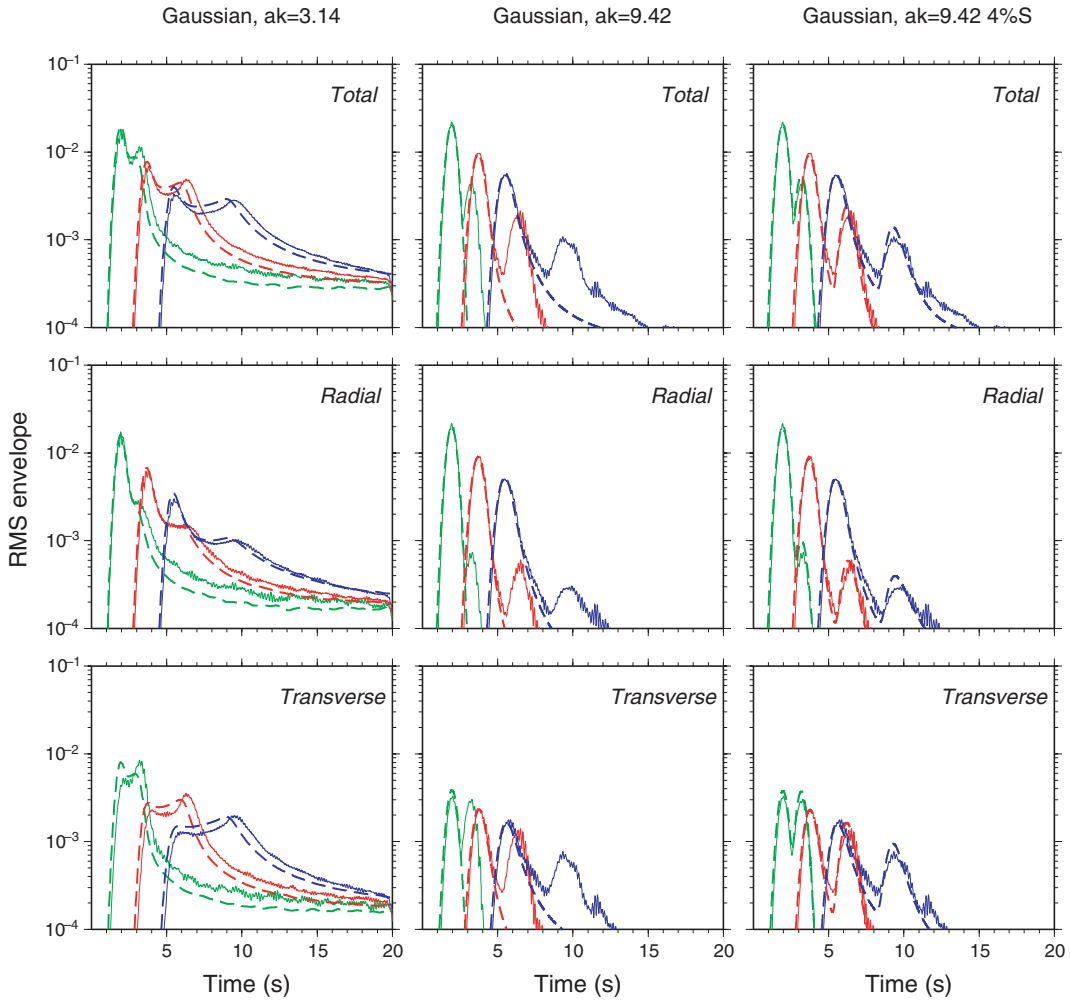

Figure 6. Same as Fig. 4, but for a medium with Gaussian ACF. An additional Gaussian bandpass filter with central frequency of 3 Hz and bandwidth of 1 Hz has been applied to the finite-difference waveforms before stack. Left: $ak = 3.14$, center: $ak = 9.42$, right: $ak = 9.42$ and 4 per cent of S energy radiation in RT.

total) component, where a clear secondary arrival is observed in the FD results that is also present but much smaller in the RT envelopes. For $ak = 3.14$, the P-wave peak on the transverse component is considerably smaller in FD than in RT. This effect is seen best at the smallest distance and diminishes with increasing distance. It points to some deficiency in the Born scattering coefficients used in RT.

There are several cases where the Born approximation breaks down. Born scattering coefficients are derived for a plane wave front incident upon a scattering volume of finite size (see Fig. 1), and they represent a far-field approximation of the scattered wave. Both assumptions may be violated if the mean free path between two successive scattering events becomes short, for example, for strong forward scattering. In this case, we would expect to find differences in pulse broadening and peak delay around the arrival time of the ballistic wave between FD and RT, but this is not observed.

Another explanation is that the initial spherical wave front has its largest curvature and highest amplitudes close to the source, resulting in different phase relations between individual scattering points in this volume. Moreover, the effective wave leaving the source volume into one specific direction is composed not only of the direct wave front but also of backscattered waves from parts of the original wave front moving in different directions. Therefore, we expect a breakdown of the angular pattern of the Born coefficients within a small distance from the source. The most notable effect will be that some shear wave energy is generated near the source, which propagates outwards in all directions. This is what we observe in the FD simulations.

In order to verify that it is indeed a near-source effect, we repeated the RT simulations with a modified source that radiates some additional S energy. Fig. 5 shows that if the source isotropically radiates about 10 per cent S wave energy, the FD envelopes can be matched with high accuracy. We emphasize that this does not mean that S energy is really generated by the source, as a similar S peak does not exist in the homogeneous medium case (Fig. 3), but that it is an effect of the medium heterogeneity, that produces some 'apparent' S-wave radiation not explained within the framework of RT and Born scattering coefficients.

In Fig. 6 the comparison for the same set of parameters is shown in a Gaussian medium. The individual FD waveforms have been bandpass filtered before the stack with a Gaussian bandpass filter, 1 Hz bandwidth, to make the envelopes more representative for a small frequency band around the central frequency of 3 Hz. In general, we find similar results as for the exponential medium, including the S-wave generation close to the source. Coda energy is

Downloaded from https://academic.oup.com/gji/article/173/2/566/728673 by guest on 16 August 2022

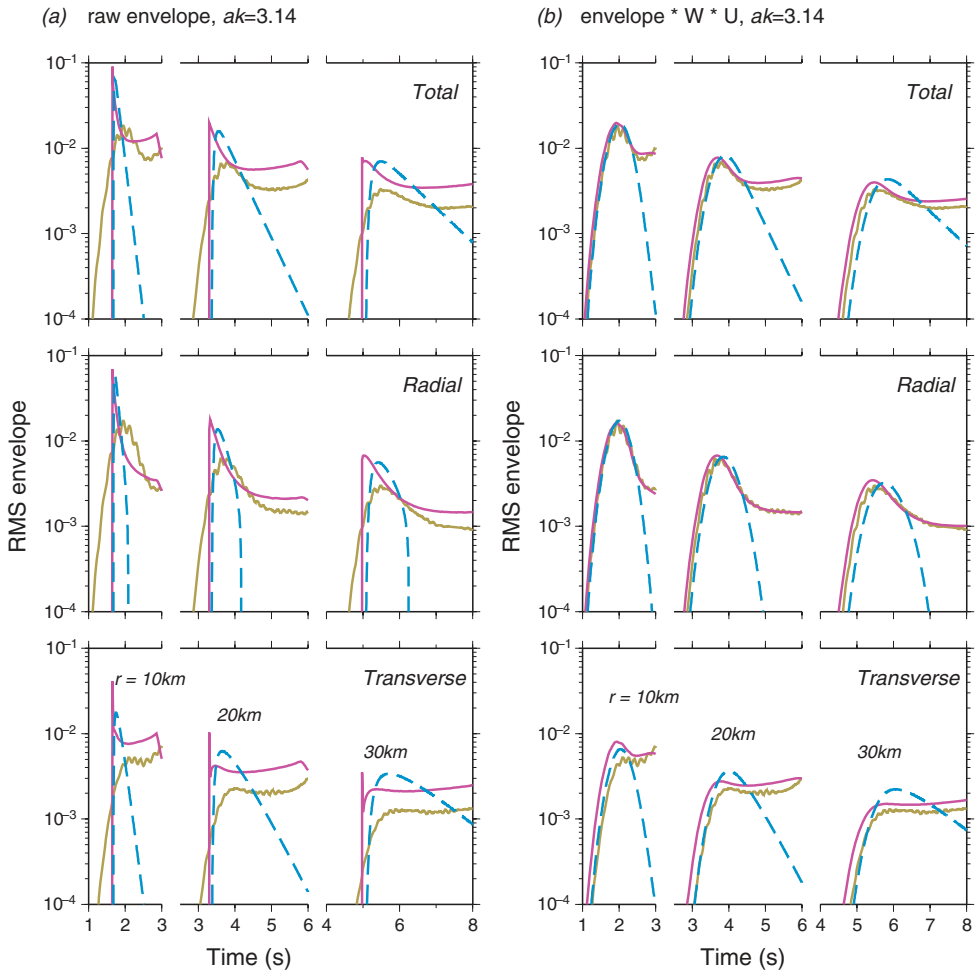

Figure 7. RT (solid purple lines) and Markov (dashed light blue lines) envelopes in a Gaussian medium with $\varepsilon = 0.1$ and $ak = 3.14$. In (a) the raw rms envelopes are plotted, in (b) envelopes are convolved with the wandering effect $w(r,t)$ (eq. 21) and the squared signal u: $u(t) = (\mathrm{d}f/\mathrm{d}t)^2$(see eq. 20). FD envelopes are plotted in for reference (olive lines).

much smaller than in exponential media; for $ak = 9.42$, the coda almost disappears. For $ak = 3.14$, coda are somewhat higher in FD than in RT. This discrepancy becomes smaller with increasing lapse time and distance from the source. A similar observation has been made previously by Przybilla *et al*. (2006) in the 2-D case. Without the bandpass filter mentioned above, the FD coda amplitude would have been even larger. In the right-hand panel of Fig. 6, we added 4 per cent of S energy radiation from the RT source. The shape of FD envelopes is then matched reasonably well.

5 COMPARISON WITH MARKOV THEORY FOR VECTOR WAVES

5.1 Markov approximation

If the wavelength is much shorter than the characteristic scale of medium heterogeneity, scattering is dominant in a small angle in the forward direction. In this case, the Markov approximation is a powerful method to directly simulate wave envelopes in random media. Recently, Sato (2007) and Sato & Korn (2007) derived analytical solutions for envelope synthesis of vector-wave envelopes in random elastic media with Gaussian ACF for isotropic radiation from a point source in two and three dimensions.

In 3-D, the intensity spectral density of P waves, $\hat{I}_0$, is obtained as (Sato 2007)

$$\hat{I}_0(r,t,\omega_\mathrm{c}) = \frac{\pi}{8t_M r^2} H\left(t - \frac{r}{\alpha_0}\right) \sum_{n=1}^{\infty} (-1)^{n+1} n^2 \left[\mathrm{e}^{-\frac{\pi^2(t-r/\alpha_0)}{4t_M}}\right]^{n^2}. \tag{23}$$

Here, $t_M = \sqrt{\pi}\varepsilon^2 r^2/(2\alpha_0 a)$ is the characteristic time, r is travel distance, ω_c is central angular frequency. The radial-component intensity spectral density is given by

$$\hat{I}_{r0}(r,t,\omega_\mathrm{c}) = \left[1 - 4\frac{\alpha_0}{r}\left(t - \frac{r}{\alpha_0}\right)\right] \hat{I}_0(r,t,\omega_\mathrm{c}) \tag{24}$$

and the transverse-component intensity spectral density by

$$\hat{I}_{t0}(r,t,\omega_\mathrm{c}) = 2\frac{\alpha_0}{r}\left(t - \frac{r}{\alpha_0}\right) \hat{I}_0(r,t,\omega_\mathrm{c}). \tag{25}$$

These quantities can be directly equated to MS envelopes, bandpass filtered around ω_c without the wandering effect (eq. 21).

5.2 Comparison of numerical results

In Figs 7 and 8, we show rms envelopes obtained from RT (solid, purple) and Markov theory (dashed, light blue) for enlarged time

Downloaded from https://academic.oup.com/gji/article/173/2/566/728673 by guest on 16 August 2022

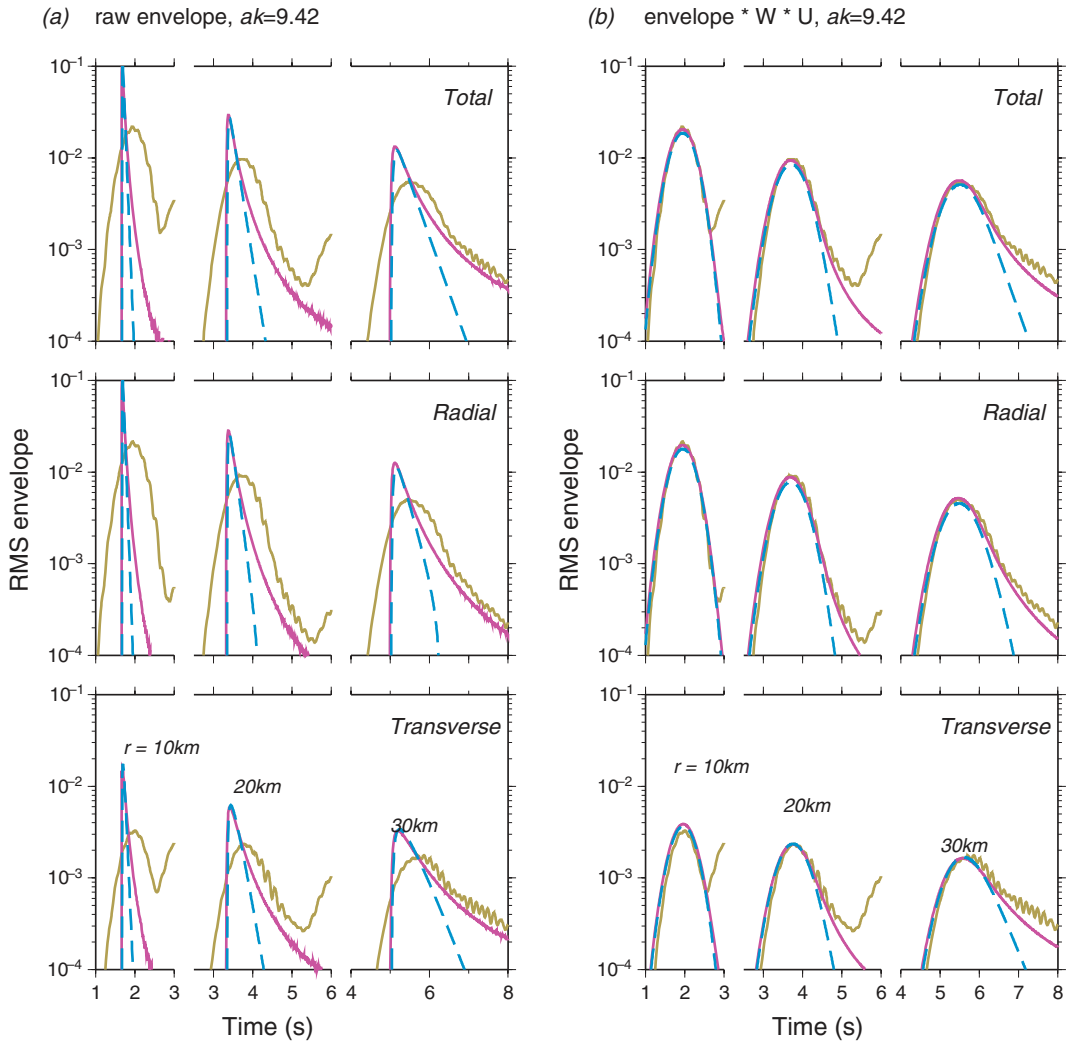

Figure 8. RT (solid purple lines) and Markov (dashed light blue lines) envelopes in a Gaussian medium with $\varepsilon = 0.1$ and $ak = 9.42$. In (a) the raw rms envelopes are plotted, in (b) envelopes are convolved with the wandering effect $w(r,t)$ (eq. 21) and the squared signal u: $u(t) = (\mathrm{d}f/\mathrm{d}t)^2$ (see eq. 20). FD envelopes are plotted for reference (olive lines).

windows around the first arrival. Figs 7(a) and 8(a) contain the raw RT and Markov envelopes without any further processing. In Figs 7(b) and 8(b), the envelopes are convolved with the squared source wavelet and the wandering effect, as previously described. We only show the Gaussian medium, as there is no analytical solution of the Markov approximation available for other types of autocorrelation functions.

For large $ak = 9.42$ Markov theory should deliver exact envelopes. In Fig. 8, there is almost perfect agreement between RT and Markov envelopes in all components except for the coda portion that is not contained in the Markov approximation. Maximum amplitude, peak decay with increasing distance and pulse broadening are correctly modelled by RT. Comparing Figs 8(a) and (b), the smoothing effect of the convolution operators for signal shape and wandering effect is clearly recognized. For reference, the FD envelopes are plotted in olive. All three results agree very well in Fig. 8(b).

For $ak = 3.14$ (Fig. 7a), the results look different. The match between RT and Markov deteriorates considerably both in pulse shape, which is broader in the Markov envelope, and in the peak arrival time, which is more delayed. The picture does not change much if wandering effect and signal width are taken into account (Fig. 7b). Although the pulse shapes of RT and Markov become more similar, there is still a clear discrepancy in the time of the maximum amplitude and in the shape and amplitude of the transverse component. The agreement between RT and FD is much better than between Markov and FD in Fig. 7(b). This clearly points to failure of the Markov approximation for small ak. We conclude that Markov approximation is only useful if $ak \geq 5$–8, that is, correlation length is larger than one wavelength.

6 CONCLUSIONS

We have developed a Monte Carlo scheme for energy transport in 3-D elastic media including P and S mode conversions. It is based on the angular-dependent scattering coefficients obtained within the Born weak scattering approximation. In contrast to similar schemes, it does not use the concept of Stokes vector but carries polarization information of S energy by using linear polarization decomposition of the scattering coefficients. This renders the numerical scheme quite intuitive. Moreover, layer boundaries with deterministic reflection and transmission, can be readily introduced by using simple energy reflection and transmission coefficients. It also seems

© 2008 The Authors, *GJI*, **173,** 566–576
Journal compilation © 2008 RAS

Downloaded from https://academic.oup.com/gji/article/173/2/566/728673 by guest on 16 August 2022

straightforward to implement multiple body-to-surface wave scattering and vice versa, if appropriate single-scattering coefficients are available. They have been recently published by Maeda *et al*. (2008).

The direction dependence of scattering becomes important if the product *ak* of wavenumber and correlation distance becomes larger than 1. Then small angle scattering around the forward direction dominates, resulting in typical effects like pulse broadening and delay of the peak amplitude. Comparison of our newly developed Monte Carlo scheme with modelling of the full 3-D elastic wavefields clearly shows that RT remains valid up to at least $ak \approx 10$. It therefore offers a unique way to model complete mean square envelopes of high-frequency wavefields in the presence of small-scale random heterogeneity starting from the first *P* onset until the late *S*-wave coda and for a wide range of correlation distances. A similar result has been found for the 2-D case by Przybilla *et al*. (2006).

A second comparison was performed against the newly developed analytical Markov approximation for vector waves in Gaussian random media (Sato 2007). It clearly showed that Markov approximation is only valid at high *ka* and quickly breaks down if *ka* becomes smaller than about 5–8. For the first time, we give an estimation for the limit of Markov approximation, which is based on comparison with full 3-D waveform modelling using FD.

While most of the smaller deviations between RT and FD envelopes can be explained by inaccuracies of the FD method like grid dispersion, anisotropy, artificial model boundaries, insufficient averaging, etc., there remains one important discrepancy. The FD simulations show some amount of *S* energy propagating away from the source that is not present either in RT or in Markov. This points to a breakdown of the approximation inherent to the derivation of the Born scattering coefficients in the vicinity of a point source. Our numerical results show that such near-source effects can cause effective shear energy radiation in the order of a few per cent ($\leq$10 per cent) of the *P* energy. We expect similar effects also for point sources with angular-dependent radiation patterns. This will require further theoretical and numerical investigations.

ACKNOWLEDGMENTS

We thank Thomas Bohlen for the permission to use his FD code. The computations have been performed at the von Neumann Computing Center at Forschungszentrum Jülich. Discussions with Ulrich Wegler, Christoph Sens-Schönfelder and Haruo Sato are gratefully acknowledged. This work was supported by Deutsche Forschungsgemeinschaft (grant Ko1068/5-1,2).

REFERENCES

Aki, K. & Chouet, B., 1975. Origin of coda waves: source, attenuation and scattering effects, *J. geophys. Res.,* **80,** 3322–3342.

Apresyan, L.A. & Kravtsov, Yu. A., 1996. *Radiation Transfer—Statistical and Wave Aspects,* Gordon and Breach, Amsterdam.

Birch, F., 1961. The velocity of compressional waves in rocks to 10 kilobars. Part 2, *J. geophys. Res.,* **66,** 2199–2224.

Bohlen, T., 2002. Parallel 3-D viscoelastic finite-difference seismic modelling, *Comput. Geosci.,* **28**(8), 887–899.

Cerjan, C., Kosloff, D., Kosloff, R. & Reshef, M., 1985. A nonreflecting boundary condition for discrete acoustic and elastic wave equations, *Geophysics,* **50,** 705–708.

Chandrasekar, S., 1960. *Radiative Transfer,* Dover Publications, New York.

Gusev, A.A. & Abubakirov, I.R., 1987. Monte-Carlo simulations of record envelope of a near eqrthquake, *Phys. Earth planet. Inter.,* **49,** 30–36.

Gusev, A.A. & Abubakirov, I.R., 1996. Simulated envelopes of non-isotropically scattered body waves as compared to observed ones: another manifestation of fractal heterogeneity, *Geophys. J. Int.,* **127,** 49–60.

Hoshiba, M., 1991. Simulation of multiple-scattered coda wave excitation based on the energy conservation law, *Phys. Earth planet. Inter.,* **67,** 123–136.

Lee, L.C. & Jokipii, J.R., 1975. Strong scintillations in astrophysics. II. A theory of temporal broadening of pulses, *Astrophys. J.,* **201,** 532–543.

Lux, I. & Koblinger, L., 1991. *Monte Carlo Particle Transport Methods: Neutron and Photon Calculations,* CRC Press, Paris.

Maeda, T., Sato, H. & Nishimura, T., 2008. Synthesis of coda wave envelopes in randomly inhomogeneous elastic media in a half space: single scattering model including Rayleigh waves, *Geophys. J. Int.,* **172,** 130–154.

Margerin, L. & Nolet, G., 2003. Multiple scattering of high-frequency seismic waves in the deep earth: PKP precursor analysis and inversion for mantle granularity, *J. geophys. Res.,* **108,** B112514,doi:10.129/2003JB002455.

Margerin, L. , Campillo, M. & Van Tiggelen, B., 2000. Monte Carlo simulation of multiple scattering of elastic waves, *J. geophys. Res.,* **105,** 7873–7892.

Modest, M.F., 1993. *Radiative Heat Transfer,* McGraw Hill, New York.

Paaschens, J.C.J., 1997. Solution of the time-dependent Boltzmann equation, *Phys. Rev. E.,* **56,** 1135–1141.

Padhy, S., Wegler, U. & Korn, M., 2007. Seismogram envelope inversion using a multiple isotropic scattering model: application to aftershocks of the 2001 Bhuj earthquake, *Bull. seism. Soc. Am.,* **97,** 222–233.

Przybilla, J., Korn, M. & Wegler, U., 2006. Radiative transfer of elastic waves versus finite difference simulations in two-dimensional random media, *J. geophy. Res.,* **111,** B04305, doi:10.1029/2005JB003952.

Rytov, S.M., Kravtsov, Y.A. & Tatarskii, V.I., 1987. *Principles of Statistical Radio Physics,* Vol. 4: Wave Propagation Through Random Media, Springer-Verlag, Berlin.

Ryzhik, L.V., Papanicolaou, G.C. & Keller, J.B., 1996. Transport equations for elastic and other waves in random media, *Wave Motion,* **24,** 327–370.

Sato, H., 1977. Energy propagation including scattering effects: single isotropic scattering approximation, *J. Phys. Earth,* **25,** 27–41.

Sato, H., 1984. Attenuation and envelope formation of three-component seismograms of small local earthquakes in randomly inhomogeneous lithosphere, *J. geophys. Res.,* **89,** 1221–1241.

Sato, H., 2007. Synthesis of vector-wave envelops in 3-D random elastic media characterized by a Gaussian autocorrelation function based in the Markov approximation: spherical wave case, *J. geophys. Res.,* **112,** B01301, doi:10.129/2006JB004437.

Sato, H. & Fehler, M, 1998. *Seismic Wave Propagation and Scattering in the Heterogeneous Earth,* Springer, New York.

Sato, H. & Korn, M., 2007. Synthesis of cylindrical vector-waves in 2-D random elastic media based on Markov approximation, *Earth Planets Space,* **59,** 209–219.

Sens-Schönfelder, C. & Wegler, U., 2006. Radiative transfer theory for estimation of seismic moment, *Geophys. J. Int.,* **167,** 1363–1372.

Shearer, P.M., & Earle, P.S., 2004. The global short-period wavefield modelled with a Monte Carlo seismic phonon method, *Geophys. J. Int.,* **158,** 1103–1117.

Weaver, R.L., 1990. Diffusivity of ultrasound in polycrystals, *J. Mech. Phys. Solids,* **38**(1), 55–86.

Wegler, U., Korn, M. & Przybilla, J., 2006. Modeling full seismogram envelopes using radiative transfer theory with Born scattering coefficients, *Pure Appl. Geophys.,* **163,** 503–531, doi:10.1007/s00024-005-0027-5.

Witte, O., Roth, M. & Müller, G., 1996. Raytracing in random media, *Geophys. J. Int.,* **124,** 159–169.

Wu, R.S., 1985. Multiple scattering and energy transfer of seismic waves—separation of scattering effect from intrinsic attenuation: I. Theoretical modeling, *Geophys. J.R. Astron. Soc.,* **82,** 57–80.

Yoshimoto, K., 2000. Monte-Carlo simulation of seismogram envelopes in scattering media, *J. geophys. Res.,* **105,** 6153–6161.

Zeng, Y., Su, F. & Aki, K., 1991. Scattering wave energy propagation in a random isotropic scattering medium I. Theory, *J. geophys. Res.,* **96,** 607–619.

Downloaded from https://academic.oup.com/gji/article/173/2/566/728673 by guest on 16 August 2022